Investigation of Novel DC Wind Farm Layout during Continuous Operation and Lightning Strikes

Rizk, Mohammad E.M.; Abulanwar, Sayed; Ghanem, Abdelhady; Chen, Zhe

Published in:
IEEE Transactions on Power Delivery

DOI (link to publication from Publisher):
10.1109/TPWRD.2020.3022853

Publication date:
2021

Document Version
Accepted author manuscript, peer reviewed version

Citation for published version (APA):
Rizk, M. E. M., Abulanwar, S., Ghanem, A., & Chen, Z. (2021). Investigation of Novel DC Wind Farm Layout during Continuous Operation and Lightning Strikes. *IEEE Transactions on Power Delivery*, *36*(4), 2221-2230. [9187861]. https://doi.org/10.1109/TPWRD.2020.3022853

This article has been accepted for publication in a future issue of this journal, but has not been fully edited. Content may change prior to final publication. Citation information: DOI 10.1109/TPWRD.2020.3022853, IEEE Transactions on Power Delivery

Investigation of Novel DC Wind Farm Layout During Continuous Operation and Lightning Strikes

Mohammad E. M. Rizk, *Member, IEEE,* Sayed Abulanwar, *Member, IEEE,* Abdelhady Ghanem, *Member, IEEE* and Zhe Chen, *Fellow, IEEE*

***Abstract*—This paper proposes a novel layout for a grid-connected DC wind farm (DCWF) and investigates the performance under continuous operation and direct lightning strikes particularly for high soil resistivity. The DCWF employs internal dc grid that supplies generated power to the host AC utility through high voltage direct current (HVDC) transmission link. The proposed layout ensures sustainability of power supply against potential interruptions of DCWFs either during normal conditions or lightning incidents to comply with grid codes regulations. During continuous operation, the proposed layout safeguards the entire DCWF cables against flow of return currents to avert derating of conductor ampacity. Besides, protects WT nacelle switchgear and entire interface converters against hazards of surge currents. Furthermore, an effective grounding system design is proposed to introduce a low impedance path for system return currents, minimize voltage drop across grounding impedance and thus maximize DCWF delivered power to the grid. A detailed system that sufficiently represents models of system cables, grounding network and interface converters is built to verify the proposed scheme significance. The obtained results assure the capability of proposed layout to cease return currents via cable sheath during continuous operation and provide superior mitigation of lightning-associated transient voltages and currents.**

***Index Terms*—DC wind farm, HVDC, Lightning strikes, grounding system, cable sheath.**

I. Introduction

INCREASING global wind power penetration entails new typologies that can handle different technical challenges and meanwhile alleviate its potential impacts on interconnected power system. Recently, extensive research on DCWFs is carried out, motivated by the rapid development of bulk power electronic converters and offshore wind power plants (WPPs) [1]–[3]. Such high power converters enable wind turbine generators (WTGs) provide dc power directly into grid via high-voltage direct current (HVDC) transmission systems [4]. DC grid is a better alternative to conventional ac counterpart where, medium frequency transformers operate at higher frequencies than ac grid frequency, which requires smaller transformer dimensions [5]–[7]. Besides, the required dc cables can transfer more power with reduced weight and size. Hence, DCWFs are foreseen highly profitable especially for offshore platforms where size, weight of installations are crucial to offer reduced overall system cost [1], [8].

Owing to their distinctive shape, remarkable height and open-air nature, wind turbines (WTs) are extensively prone to recurrent direct lightning strikes [9]. Such strikes not only cause damage to WTs blades and structure, but also to low-voltage control circuits and surge arresters [10]. More than 50% of WT common failures caused by lightning strikes are due to low-voltage control and communication circuits breakdowns [11]. Such challenges may lead to increased WTGs downtime that would increase operation cost and indeterminacy of wind farms (WFs) power generation. Hence, lightning protection measures are imperative to safeguard WTs physical structure, human operators and maintain WFs grid connected to fulfill grid code obligations.

Typically, multipoint sheath grounding is recommended to avoid serious voltage buildup along the cable length with electromagnetic transients. During normal operation in alternating current WFs (ACWFs), the generated three-phase currents are balanced through the cable cores, so, almost no current returns through the grounded cable sheath. On the other hand, grounding the cable sheath in DCWFs imposes the core current to return via the sheath which not only derates conductor ampacity, but also degrade both inner (main) and outer insulation layers of the cable. This is because the ampacity of the cable sheath is considerably lower than that of its core. Therefore, the current returns typically through the ground in DC systems.

Grounding system is crucial to effectively protect WT physical structure, nacelle switchgear and control cabinets against transient overvoltages via providing a low impedance path (below 10 Ω at low frequencies) into earth for surge currents [11], [12]. However, due to growing demand on wind energy, WFs may be sited at suboptimal territories having high soil resistivity that raises serious concerns about the grounding system efficacy [13], [14]. Poor grounding system (*i.e.,* high grounding impedance) causes serious ground potential rise (GPR), and subsequently detrimental electrical stresses on power system apparatus and humans [**?**]. In this context, return dc currents result also in a considerable voltage drop across the local grounding system (LGS) of each WT. Consequently, the delivered power to the grid decreases drastically that represents wasteful DCWF layout.

Simplified models for WTGs and their control structures are usually adopted when investigating lightning strikes impacts on WFs [10]. This paper presents a detailed model for WTGs and their control in a grid-connected onshore DCWF to

Manuscript received .

M. E. M. Rizk, S. Abulanwar and A. Ghanem are with the Department of Electrical Engineering, Faculty of Engineering, Mansoura University, Mansoura 35516, Egypt (e-mails: eng_mohammad_2007@mans.edu.eg, abulanwar@mans.edu.eg and aghanem_m@mans.edu.eg)

Z. Chen is with the Department of Energy Technology, Aalborg University, 9220,Aalborg, Denmark, (e-mail: zch@et.aau.dk)

provide insight into transient voltages and currents of WTG. A novel DCWF layout is also proposed and investigated under regular operation and lightning strikes considering poor grounding system. The novel layout integrates benefits of multiple solid grounding the sheath (to suppress lightning-transient overvoltages) and also opening the sheath from one end (to remove return path of WTG currents through sheathes during continuous operation).

The major contributions of this paper are: 1) Safeguarding DCWF entire cables from excessive currents flowing in the sheathes that can cause frequent interruptions, which to the best of our knowledge, has not been addressed before. 2) A proposed layout reliant on installing surge arresters over horizontal and vertical cables sheathes of the entire DCWF to force WTG currents to return through grounding system rather than cable sheath and meanwhile mitigate sheath overvoltage incurred by lightning strike; 3) An effective grounding system design is presented and validated for higher soil resistivity to ensure human safety and vital equipment using a network of counterpoises connecting local grounding of each WT and/or converter; 4) Detailed model that properly characterizes not only for WTG realistic models and controls but also the transient behavior for practical grounding configuration and arresters; and 5) The proposed scheme is suitable for other WTG and can be applied for offshore platforms to protect entire cables from excessive sheath currents.

Different schemes are also investigated to evaluate the significance of the proposed scheme in providing a proper regular operation and an effective protection against lightning strikes as well. The rest of this paper is organized as follows, Section II introduces description of the proposed protection scheme with control structure. Time-domain simulations that verify the proposed scheme is provided in section III. Section IV concludes the paper.

II. Proposed Protection Scheme Structure

This section presents the proposed layout which incorporates design and modeling of surge arresters, effective grounding system and WTG control structure.

A. System Description and Modeling

Fig. 1 depicts the proposed structure of a grid-connected DCWF via an HVDC transmission system. The DCWF consists of two identical strings employing full-scale permanent magnet synchronous generators (PMSG) WTs, each is rated at 5 MW with 50 MW net capacity. Each WTG comprises PMSG, full-scale active rectifier to regulate the generated power and a dc/dc converter that maintains the WTG dc link voltage constant, $V^*_{dc,i}$ = 5 kV irrespective of the delivered power. The whole WTs deliver their power through vertical single-core cables through their towers, and attached via radially paralleled underground single-core dc cables to the dc/dc collector side converter (CSC) which is devoted to regulate the collector voltage at nominal value, V^*_{cc} = 30 kV. The DCWF harvested power is transmitted via 500 km HVDC link with a rated voltage, V^*_{hvr} = 300 kV dictated by a dc/ac two level pulse-width modulated (PWM) grid-side converter (GSC) which can also regulate the exchanged reactive power with the grid to attain a desired power factor. Since high power dc/dc converters are key equipment for realization of DCWF, parallel connected single active bridge (PCSAB) unidirectional dc/dc converter configuration is adopted in this paper. Such converters request smaller filtering inductors and are favorable for DCWFs especially for offshore scenarios due to high fault current tolerance, lower maintenance cost [1]. Details about such converters modeling, control and design are found in [2].

The grounding system employs a network of counterpoises extending above underground cables and connecting LGSs of WTs as shown in Fig. 1. Those counterpoises reinforce the entire grounding system, render a low impedance path for surge currents. Thus, minimizing GPR, avoiding considerable power loss, and maximizing the DCWF efficiency significantly. Despite using counterpoises, a greater portion of current returns through multipoint grounded sheath as compared to counterpoise owing to its lower characteristic impedance; this overheats the cable sheath and thereby impairs the cable. Accordingly, it is proposed to install two groups of sheath-connected arresters that are $(\mathrm{SA_{vs}}$ and $\mathrm{SA_{hs}})$ on the vertical and underground cables as shown in Fig. 1. Primarily, these arresters protect the cable during regular conditions via forcing currents to return through grounding network rather than cable sheath. Moreover, provide a protection for the cable against lightning incidents by damping transient overvoltages upon the cable sheath. Thus, maximizing DCWF cables lifetime and reducing potential interruptions for all conceivable conditions. $\mathrm{SA_{vs}}$ ceases each WTG current to return through its vertical cable sheath during normal operation, and discharges surge currents irritated by lightning strikes into the grounding system. $\mathrm{SA_{hs}}$ restrains surge voltages evoked by lightning currents on the underground cable sheath to protect both outer and inner insulation. Core-connected arresters $(\mathrm{SA_c})$ is typically installed at each WT hub and CSC to alleviate surge voltages impact on vertical cables and power converters.

B. WT Tower and Lightning Return Stroke Models

WT tower is represented by distributed parameters model due to its considerable height where the per unit length parameters are given by (1) assuming a vertical cylinder [15].

$$L_T = \frac{\mu_o}{2\pi \ln\left((h/r)-1\right)} \quad , \qquad C_T = \frac{2\pi\varepsilon_o}{\ln\left((h/r)-1\right)} \tag{1}$$

L_T and C_T are respectively the per-unit length inductance and capacitance in $\frac{\mathrm{H}}{\mathrm{m}}$ and $\frac{\mathrm{F}}{\mathrm{m}}$; the tower height is h = 90 m and $r = \frac{D_t+D_b}{4}$ is its mean radius where the diameters at the tower top and bottom are respectively D_t = 4 m and D_b = 6 m [16].

Fig.2 shows the current waveforms at the lightning channel base that are expressed by Heidler's function, given by (2), for both first and subsequent strokes, denoted by (FRS) and (SRS). Table I gives their Heidler's coefficients [17], [18]. The lightning channel impedance is assumed to be 800 Ω [19].

$$I_{RS}(t) = \sum_{k=1}^{K} \frac{(I_{ok}/\eta_k)\cdot \exp(-t/\tau_{2k})\cdot (t/\tau_{1k})^{n_k}}{1+(t/\tau_{1k})^{n_k}} \tag{2a}$$

$$\eta_k = \exp\left(-\left(\tau_{1k}/\tau_{2k}\right)\cdot \left(n_k \cdot \tau_{2k}/\tau_{1k}\right)^{-n_k}\right) \tag{2b}$$

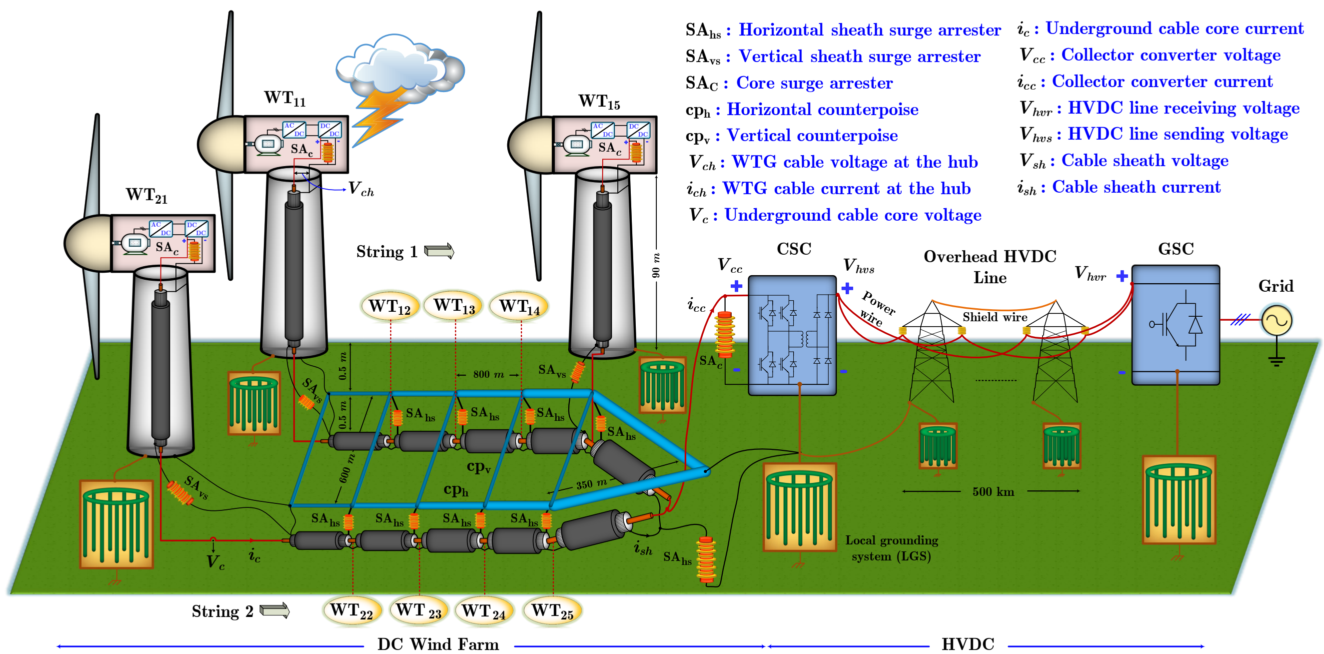

Fig. 1. DC Wind farm layout with proposed protection scheme.

TABLE I
HEIDLER'S COEFFICIENTS FOR FRS AND SRS

	FRS								SRS	
k	1	2	3	4	5	6	7	8	1	2
I_{0k} (kA)	6	6	5	5	8	17	17	12	10.7	6.5
n_k	2	2	3	5	9	30	2	14	2	2
τ_{1k} (μs)	2	3	3.5	5	6	7	70	12	0.25	2.1
τ_{2k} (μs)	100	76	10	30	26	23.5	200	26	2.5	230

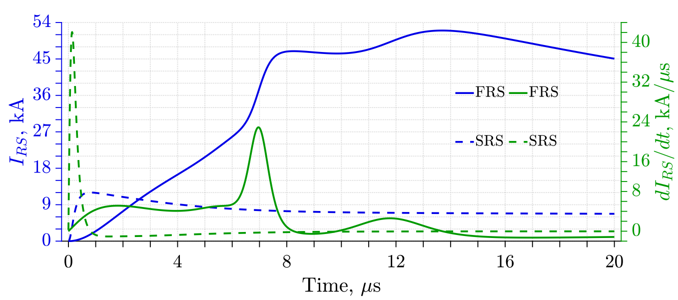

Fig. 2. Current waveforms of FRS and SRS with their time-derivatives.

C. Grounding System Model

For normal operation of DCWFs, power delivery and voltage levels are significantly influenced by the grounding system design because of the returning currents. Moreover, the proper design of the grounding system is essential to ensure an effective protection against lightning overvoltages in WFs, in particular with high soil resistivity [13], [20]. In this study, DCWF grounding system comprises LGS at each WT, CSC, and GSC as well as a grid of counterpoises connecting the local grounding systems of the entire WF and the CSC together. Two values of soil resistivity, ρ_1 = 500 and ρ_2 = 2000 Ωm are considered to investigate the influence of ρ on both normal operation and lightning electromagnetic transients in DCWFs. The relative permittivity of soil is considered as ε_r = 10.

1) Local Grounding System (LGS): The LGS comprises nine vertical grounding electrodes that are circularly arranged on a diameter of 10 m as shown in Fig. 1. The length and radius of each electrode are respectively 6 m and 2 cm. Fig. 3a shows the equivalent circuit utilized to represent the transient behavior of the LGS [21]. The LGS is simulated using the finite-difference time-domain (FDTD) method where the SRS current is injected into the LGS and the resulting GPR is computed. Afterwards, the parameters L_g, C_g, and R_g that well match the FDTD-computed GPR are determined to be 0.1 μH, 4 nF, and 19.8, 67.6 Ω for ρ_1, ρ_2, respectively [22], [23]. The SRS is used to determine the equivalent circuit parameters owing to its higher di/dt and consequently higher frequency content as compared to the FRS current waveform. Figs. 3c, 3e compare DC and transient models of the LGS with the FDTD simulation. Parameters L_g and C_g are eliminated in the DC model. It is obvious from Fig. 3 that the transient model well conforms to FDTD simulations as compared to the DC model, in particular with higher ρ.

2) Counterpoise: The counterpoise is a bare buried wire under a depth of 0.5 m connecting the LGSs in the entire DCWF as shown in Fig. 1. Since the counterpoises length is in terms of hundreds of meters, the traveling time of propagating lightning-electromagnetic pulses through them should be considered. Consequently, a distributed model for the counterpoise is implemented in this study where the per unit length parameters of the counterpoise shown in Fig. 3b are given by (3) [21]. The current dispersion into earth depends mainly on G_{cp} of the counterpoise. However, EMTP software doesn't support the distributed G_{cp}. Therefore, the distributed r_{cp}, L_{cp}, and C_{cp} are divided into small segments whereas the G_{cp} is divided on those segments (equivalent to multi-Π model.) To validate this approach, the counterpoise is simulated using the FDTD method where the SRS current waveform is injected and voltage buildup is computed at 100 m away from the injection point. Figs. 3d, 3f illustrate the computed buildup voltage considering different segments, namely, 100, 50, and 25 m. As shown, the 25 m segment matches the FDTD-computed results well. Lengths of counterpoises are shown in Fig. 1 whereas their radii are selected according to the current returning through each section.

$$r_{cp} = \frac{\rho}{A_{cp}}\ ,\quad L_{cp} = \frac{\mu_o A_0}{2\pi}\ ,\quad C_{cp} = \frac{\pi\varepsilon}{A_0}\ ,\quad G_{cp} = \frac{\pi}{\rho A_0} \tag{3}$$

where $A_0 = \ln\left(\frac{2\ell}{\sqrt{2ad}}\right) - 1,\ \ell \gg a, d;\ \rho,\ A_{cp},\ \ell,\ a$ stand for counterpoise resistivity, cross-section area, length and radius respectively. d is the burial depth, ε is the soil permittivity.

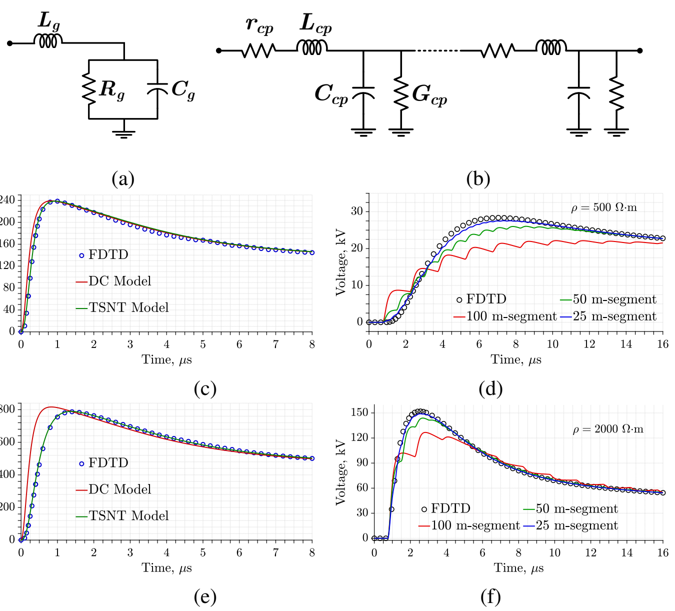

Fig. 3. Grounding system model and validation. (Left column: LGS; right column: counterpoise.) (a), (b) Circuit model; model validation with SRS current waveform at ρ =: (c), (d) ρ_1 = 500 Ωm, and (e), (f) ρ_2 = 2000 Ωm.

D. Cables and overhead line Models

Fig. 4 shows the single-core cable used in the DCWF as vertical cables through the WT towers or underground cables between WTs and the CSC (30 kV cables.) The underground cables are placed under 1m depth as shown in Fig. 1. Those cables are modeled using the frequency-dependent model in PSCAD/EMTDC software. Cables dimensions are obtained from [24] and given in Table II. As implied from Table II, the single core cables are selected based on the voltage level (determined by the main insulation thickness, th_{ins_1}) and also the current capacity of each cable section (determined by the cross-section area of the core, A_c). The thickness of both semi-conductor layers shown in Fig. 4 has been determined from D_{co}, th_{ins_1} and D_{ins_1}. HVDC link between CSC and GSC is 500 km overhead line with multiple transmission towers distanced by 400 m. Five towers are only considered from both CSC and GSC because of the great length of the line. The height and radius are respectively 38 m and 2 cm for the power line; 52 m and 8 mm for the shield wire whereas they are also modeled using the frequency-dependent model. The transmission towers are modeled following [16].

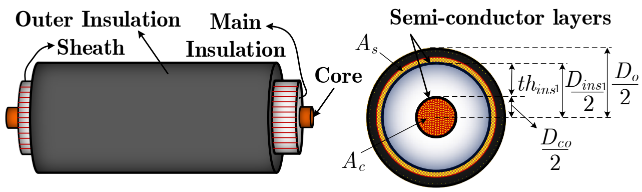

Fig. 4. Configuration of the Single-core cable used in the DCWF.

TABLE II
GEOMETRIC DIMENSIONS OF SINGLE-CORE CABLES IN DCWF

Cable Section	A_c $(mm)^2$	D_{co} (mm)	th_{ins_1} (mm)	D_{ins_1} (mm)	A_s $(mm)^2$	D_o (mm)
$WT_{\substack{1\\2}1} \rightarrow WT_{\substack{1\\2}2}$ *	95.0	11.2	8.0	28.8	25.0	37.0
$WT_{\substack{1\\2}2} \rightarrow WT_{\substack{1\\2}3}$	185.0	15.8	8.0	33.4	35.0	42.0
$WT_{\substack{1\\2}3} \rightarrow WT_{\substack{1\\2}4}$	400.0	23.2	8.0	40.8	35.0	51.0
$WT_{\substack{1\\2}4} \rightarrow WT_{\substack{1\\2}5}$	630.0	29.8	8.0	48.0	35.0	58.0
$WT_{\substack{1\\2}5} \rightarrow$ CSC	1000.0	37.9	8.0	56.1	35.0	67.0

* The vertical cables extending through the WT towers are the same as both underground cable sections from $WT_{\substack{1\\2}1}$ to $WT_{\substack{1\\2}2}$.
* $WT_{\substack{1\\2}1}$ refers to WT_{11} and WT_{21}.

E. Surge Arrester Model

Typically, arresters are frontline protection against transient overvoltages. They comprise discs of Zinc-Oxide that have nonlinear (V-I) characteristics. The arrester operating voltage is proportional to the number of discs. At normal voltage levels, the current flowing through arresters is almost zero while it sharply increases when voltage exceeds allowable levels; thus suppressing transient overvoltages. As aforementioned, two distinct arresters of different operating voltages according to where they are connected are incorporated. In the WT hub, SA_c is connected between the core of vertical down-cable and the grounded WT tower as shown in Fig. 1. Moreover, SA_{hs} is connected between the underground cable sheath and the grounding system while SA_{vs}, is installed between the bottom-end of the vertical cable sheath and the grounding system as shown in Fig. 1. Fig. 5a shows the transient model that has been proposed in [25] and adopted to represent both SA_s and SA_c. The (V-I) characteristics of the nonlinear resistors A_0 and A_1 are shown in Fig. 5b for both core and sheath arresters (SA_c and SA_s). In addition, L_0 and L_1 are calculated as given by (4) where R_o is assumed by 1 MΩ. The electrical data for SA_s and SA_c are given in [26] as follows 1) rated voltage: U_n = 5 and 37.5 kV_{rms}; 2) operating continuous voltage: U_c = 4 and 30 kV_{rms}; 3) residual voltages for a steep current impulse

This article has been accepted for publication in a future issue of this journal, but has not been fully edited. Content may change prior to final publication. Citation information: DOI 10.1109/TPWRD.2020.3022853, IEEE Transactions on Power Delivery

of 10 kA$_{peak}$ and 1 μs rise time and T_2 tail time: $U_{r(1/T_2)}$ = 13.2 and 99 kV$_{max}$; and 4) residual voltages for a lightning current impulse of 10 kA$_{peak}$ and $8/20$ μs: $U_{r(8/20)}$ = 12 and 90 kV$_{max}$, respectively. These data are used to determine the model parameters as elaborated in [25]. The rated energy of arrester is estimated by 10 kJ/kV of operating continuous voltage at 40 °C.

$$L_1 = \frac{(U_{r(1/T_2)} - U_{r(8/20)})}{4 \cdot U_{r(8/20)}} \cdot U_n \quad , \qquad L_0 = \frac{L_1}{3} \tag{4}$$

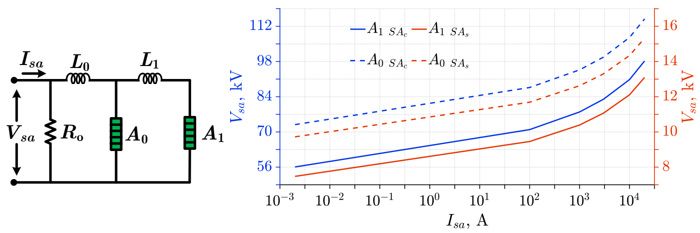

(a) (b)

Fig. 5. Surge Arrester: (a) equivalent circuit, and (b) IV characteristics.

F. WTG Model and Controls

Detailed modeling and control of variable-speed WTs is extensively studied [27], [28], so a brief description is introduced. Normally, WT is controlled to attain maximum power point tracking (MPPT) by continually adjusting rotor speed to maintain optimal tip-speed ratio λ_{opt} in response to wind speed variation. Hence, maximum captured power is given by (5) where, A is the blades swept area, R is the blade radius, C_p is rotor aerodynamic coefficient [27].

$$P_{max} = \frac{A \cdot R \cdot C_{p-max}}{2 \cdot \lambda_{opt}^3} \cdot \omega_r^3 \tag{5a}$$

$$C_p = 0.22 \cdot (116 \cdot \sigma - 0.4 \cdot \beta - 5) \cdot \exp(-12.5 \cdot \sigma) \tag{5b}$$

$$\sigma = (\lambda + 0.08 \cdot \beta)^{-1} - 0.035(\beta^3 + 1)^{-1} \tag{5c}$$

The model of salient-pole PMSG without dampers is given by (6) in a rotating dq synchronous reference frame [28], [29].

$$\frac{m_d V_{dc,i}}{2} = R_s i_{sd} + (L_{md} + L_{ls})\dot{i}_{sd} - \omega_r (L_{mq} + L_{ls}) i_{sq} \tag{6a}$$

$$\frac{m_q V_{dc,i}}{2} = R_s i_{sq} + (L_{mq} + L_{ls})\dot{i}_{sq} + \omega_r \big((L_{md} + L_{ls}) i_{sd} + \psi_f\big) \tag{6b}$$

$$\frac{2J}{P}\dot{\omega}_r = \Big(T_m - \frac{3P}{4}\big((L_{md} - L_{mq}) i_{sd} + \psi_f\big) i_{sq}\Big) \tag{6c}$$

where, m_d, m_q stand for machine-side converter modulating signals, $V_{dc,i}$ PMSG dc link voltage, R_s is the stator resistance, L_m, L_{ls} are mutual and leakage inductances, i_{sd}, i_{sq} direct and quadrature stator current components, ω_r is the electrical rotor speed, ψ_f is the permanent magnet flux, P is the number of machine poles, J is the lumped inertia of WT and rotor and T_m is the WT mechanical torque.

Each PMSG employs two respective converters, *i.e.,* full-scale active rectifier to regulate the machine for various wind speeds and wind generator dc/dc converter WGC to deliver the captured power to the dc collector. As dc/dc converters are essential portion of DCWF, system dc converters are modeled as PCSAB unidirectional dc/dc converter to provide high dynamic performance during transients [1], [2]. A control structure of the DCWF and HVDC converters is depicted in Fig. 6a. The dc link voltage of each PMSG, $V_{dc,i}$ is regulated by its respective WGC via acting on its output dc current $i_{dc,i}$, where the controller output determines the switching signal of the converter. Similarly, CSC dictates the dc collector voltage V_{cc} via controlling its dc output current i_{cc}. The HVDC receiving-end voltage V_{hvr} is manipulated by GSC which also regulates the exchanged reactive power with the grid through manipulating grid side i_{dqg} currents to achieve a desired power factor according to grid code regulations. Fig. 6b shows a linearized block diagram of voltage control of each dc/dc converter that obtains the optimal parameters of PI controller using symmetrical optimum design approach [1], [2]. Hence, each converter input capacitance can be determined so as to restrict the peak capacitor voltage overshoot in response to step change of its respective input current.

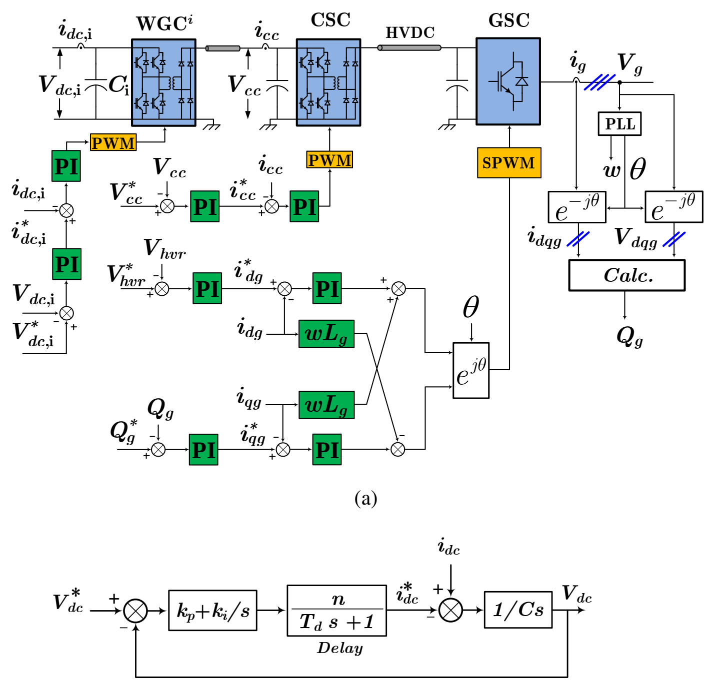

(a)

(b)

Fig. 6. Controller structure (a) Interface converters control structure, and (b) Linearized input voltage dc converter controller.

III. Case Studies

A. Continuous Operation

Fig. 7 depicts structure of the proposed scheme at WT$_{15}$ where arresters (SA$_{hs}$, SA$_{vs}$) are installed on sheathes of both vertical cables, and horizontal underground cables to ensure cables protection against lightning incidents at the WT hub. The sheath of the vertical cables is connected to the sheath of the underground cables via SA$_{vs}$ whereas the sheath of

This article has been accepted for publication in a future issue of this journal, but has not been fully edited. Content may change prior to final publication. Citation information: DOI 10.1109/TPWRD.2020.3022853, IEEE Transactions on Power Delivery

the underground cables are grounded via SA_{hs}. For scheme-1, those SA_{hs}, SA_{vs} are short-circuited while they are open-circuited for scheme-2. Table III summarizes structure of all investigated schemes at different locations in the DCWF to verify the effectiveness of the proposed scheme (scheme-3). Fig. 8 illustrates DCWF performance at WT_{15} during continuous operation for different practical operational schemes. As the voltage is controlled at the CSC, all schemes almost behave similarly and the voltage is maintained at the reference set value (Fig. 8a) even with different soil resistivities. Owing to the fact that the characteristic impedance of the cable sheath is lower than that of counterpoise, in scheme-1, most of the current returns through the sheath as shown in Fig. 8c. On contrary, Fig. 8c shows also that zero sheath-current is guaranteed either due to opening sheath termination (scheme-2) or connecting SA_{hs}, SA_{vs} to the sheath ends (schemes-3). On the other hand and without counterpoise, the DCWF entire voltage rises during normal operation owing to the higher grounding resistance for schemes-2 and 3 while scheme-1 is unaffected as shown in Fig. 8b. This is owing to the solidly grounded sheath which permits the flow of return current as seen in Fig. 8d. The considerable voltage drop across the high grounding impedance particularly for ρ_2 reduces the DCWF generated currents as shown in Fig. 8d resulting in remarkable power loss. It is worth to mention that without counterpoise, the only return path for the WT generated current i_{ch} is the LGS for schemes-2 and 3 as shown in Fig. 8d. Accordingly, a considerable GPR arises on the LGS of CSC because of the returning currents. This potential rise triggers the SA_{hs} connected to sheath ends at the CSC side for scheme-3 as shown in Fig. 9; this SA_{hs} draws a higher continuous current especially for ρ_2 which deteriorates it. Fig. 10 shows i_{ch} for schemes-2 and 3 without counterpoise where both schemes experience identical behavior except for WT_{11} with scheme-3. This is due to the current flowing through the SA_{hs} connected at the CSC returns to both WT_{11} and WT_{21} owing to solidly grounding the sheath at their terminals (see Fig. 1). Additionally, it is clear that i_{ch} is significantly lower without counterpoise for ρ_2 as compared to ρ_1 for both schemes which dramatically reduces the net delivered power to the grid.

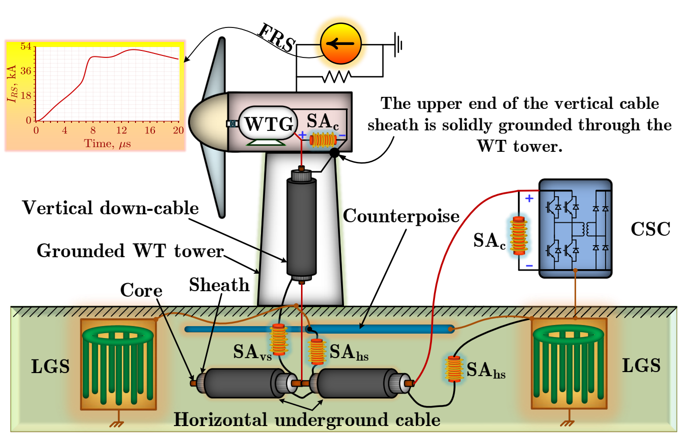

Fig. 7. Structure of sheathes connections of proposed scheme at WT_{15}

TABLE III
INVESTIGATED SCHEMES FOR CABLE SHEATH GROUNDING

Scheme	Underground cable sheath end at CSC	Sheath ends at $WT_{1\frac{1}{2}2} \rightarrow WT_{1\frac{1}{2}5}$ * underground cable	vertical down-cable
1	solidly grounded	solidly grounded	solidly grounded
2	opened	opened	opened
3	**grounded via SA_{hs}**	**grounded via SA_{hs}**	**connected to SA_{vs}**
4	grounded via SA_{hs}	grounded via SA_{hs}	opened
5	grounded via SA_{hs}	opened	connected to SA_{vs}

* At $WT_{1\frac{1}{2}1}$, sheath ends of underground cables are solidly grounded for the whole schemes.

B. Influence of Horizontal and Vertical arresters

Despite schemes-4,5 can effectively provide proper normal operation as scheme-3, their performance during lightning incidents will be deficient. Fig. 11 reflects system performance following a lightning strike at WT_{15} under schemes-3,4,5. As seen, the proposed scheme (schemes-3) provides superior mitigation of transient underground core as well as sheath voltages that could be destructive for cable insulation and also transient currents at the CSC. The depicted results reveal the effectiveness of SA_{vs} and SA_{hs} employed in the proposed scheme. Thereafter, system response to lightning strikes will be examined in light of scheme-3 against schemes-1,2 which are common practices for protection from surges.

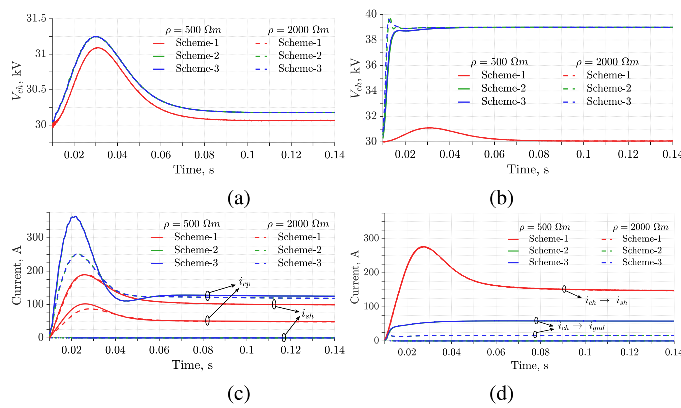

Fig. 8. Normal operation results at WT_{15}. (Left column: with counterpoise; right column: without counterpoise.) (a), (b) V_{ch}; (c), (d) currents

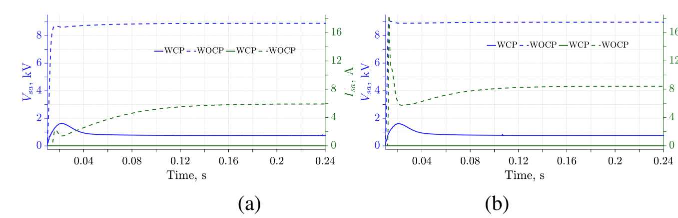

Fig. 9. Scheme-3 sheath arrester at CSC results during normal operation without counterpoise: (a) ρ_1 = 500 Ωm , (b) ρ_2 = 2000 Ωm

C. System Behavior Under Lightning Strikes

Figs. 12-18, demonstrate system behavior under FRS to WT_{11}, WT_{15} of string 1 considering both ρ values. Subsequent to the surge incident at the tower, voltage swell over the

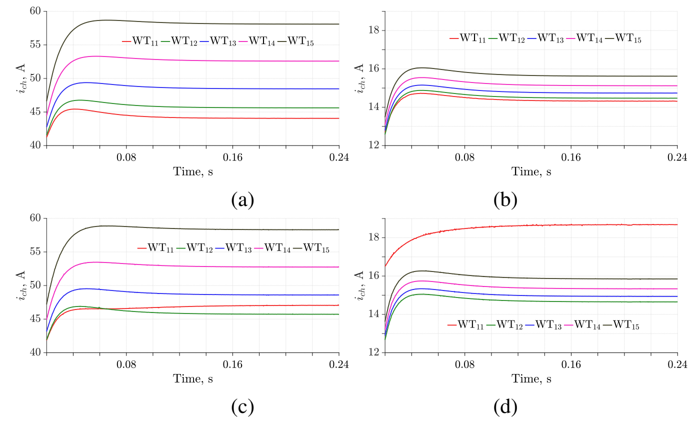

Fig. 10. String1 WT generated currents during normal operation without counterpoise. (Left column: ρ_1; right column: ρ_2.) (a), (b) Scheme-2; (c), (d) Scheme-3

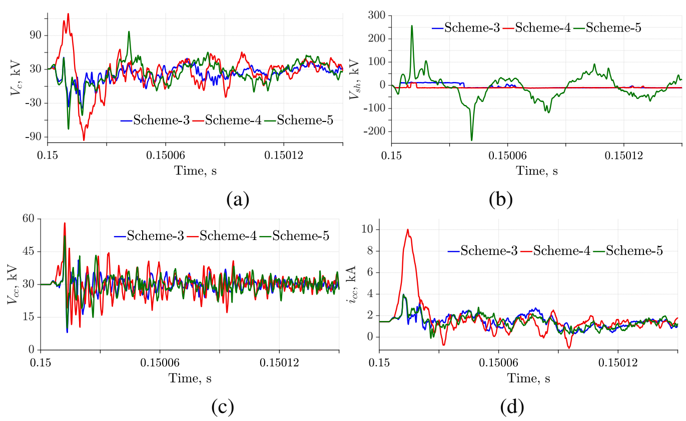

Fig. 11. Typical results for lightning strike at WT_{15} for ρ_1: (a) V_c , (b) V_{sh}, (c) V_{cc} and (d) i_{cc}

vertical cable core engages hub arresters to discharge; the peak voltage detected over all WTs, V_{ch}, is shown in Fig. 12. The voltages of the non-struck string also increases causing the entire WF arresters to operate as seen in Fig. 13. Consumed energy E_{sa} under scheme-2 is higher especially for ρ_2. In addition to Fig. 13, Table IV also demonstrate the values of E_{sa} consumed in $\mathrm{SA_c}$. The hub arresters ($\mathrm{SA_c}$) suppress surge voltages in their vicinity. Nevertheless, voltage at the underground cable, V_c in the entire WF seriously increases as depicted in Fig. 14. The worst situation results for FRS to WT_{11} where voltage reaches ≈ 300 kV at the struck tower and ≈ 119 kV at WT_{21} (nearest to WT_{11} due to vertical counterpoise) which would be ruinous for cables insulation. Consequently, higher transient core currents, i_c arise as seen in Fig. 15 that exceeds 7 kA at the struck WT_{15}, ρ_2. However, schemes-1,3 provide effective mitigation as compared to scheme-2 due to introducing a discharging path to the ground.

Sheath voltages, V_{sh} measured at each junction between WT vertical and underground cable are illustrated in Fig. 16. As the lightning directly strikes the grounded tower, sheath voltage is considerably affected under scheme-2 as compared to schemes-1,3. As seen, voltage over the sheath reaches values close to 400 kV for ρ_2 and 175 kV for ρ_1 considering scheme-2 for strike at WT_{11}. Grounding the sheath (scheme-1) ensures minimal sheath transient voltage, yet, permits flow of return currents as previously discussed. Conversely, scheme-2 yields lower surge currents in the sheath compared to that in schemes-1,3 at the onset of lightning incident as illustrated in Fig. 17. However, these transient currents are rapidly attenuated owing to multipoint sheath grounding (schemes-1) and establishing grounding channel due to sheath-connected arresters (scheme-3) which also effectively relief sheath buildup voltage. Fig. 18 shows E_{sa} of the suggested horizontal and vertical $\mathrm{SA_s}$ ($\mathrm{SA_{hs}}$, $\mathrm{SA_{vs}}$). Beside Fig. 18, Table V demonstrates the consumed energy for sheath-connected arresters $\mathrm{SA_s}$. Generally speaking, E_{sa} is much lower than the thermal capacity of these arresters as inferred from Subsection II-E. Accordingly, proposed $\mathrm{SA_s}$ lifetime will be longer, so that scheme-3 offers fairly quick payback. Besides, Fig. 18b, 18d implies that profile of E_{sa} of the non-struk string is highest at WT_{25} and lower at WT_{21} irrespective of strike location. This can be attributed to the lower surge impedance of sheath compared to that of counterpoise, thus most of the surge current flows radially via the sheath from the struck WT to the other WTs in the same string towards CSC.

Consequently, Scheme-3 is inevitable to protect system cables against flow of excessive currents via sheathes which can ruin cables insulation during continuous operation. Also, ensures minimum sheath build up voltage following lightning strikes especially when ground resistivity is poor.

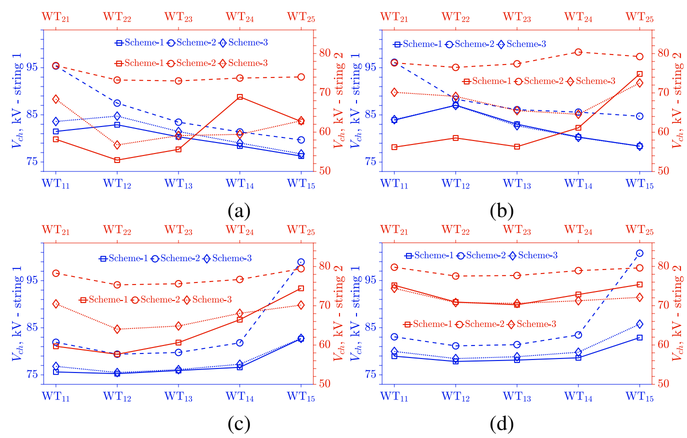

Fig. 12. Waveforms of V_{ch}. (Left column: ρ_1; right column: ρ_2.) (a), (b) FRS to WT_{11}; (c), (d) FRS to WT_{15}.

IV. Conclusion

This paper proposes an effective novel design of grid-connected DCWF and analyzes the performance under both regular operation and lightning strikes in light of poor grounding systems. Typically, multipoint sheath grounding in AC systems is a common practice for long cables to ensure minimal potential over cable run during lightning invasion. In DCWFs, such a practice (scheme-1) allows the generated currents to constantly flow via sheath thus exceeding conductor ampacity and destroying the cable. While opening cable sheath termination (scheme-2) can adequately cancel flow of return current through it, serious transient voltages emerge during lightning incidents. A layout that combines benefits of both schemes is proposed in this paper. The central premise of the suggested layout relies on connecting sheath-connected

This article has been accepted for publication in a future issue of this journal, but has not been fully edited. Content may change prior to final publication. Citation information: DOI 10.1109/TPWRD.2020.3022853, IEEE Transactions on Power Delivery

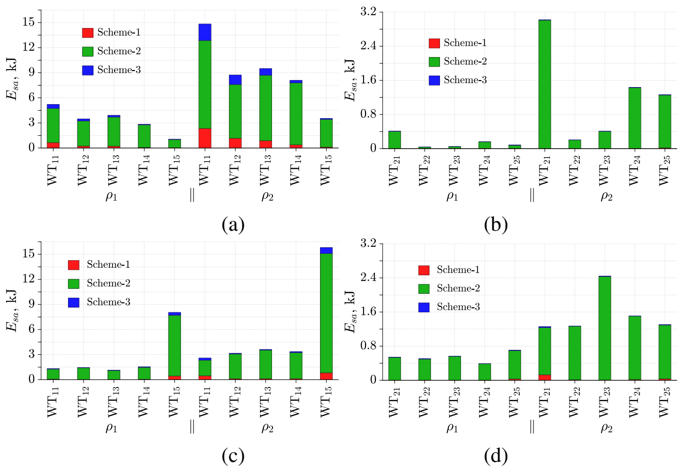

Fig. 13. E_{sa} of hub arresters SA_c. (Left column: string-1; right column: string-2) (a), (b) FRS to WT_{11}; (c), (d) FRS to WT_{15}.

TABLE IV
ENERGY CONSUMED, E_{sa} IN (KJ) FOR SA_C AT WT HUB. ($E_{sa-\rho_1}$ / $E_{sa-\rho_2}$)*

FRS	WT_{11}			WT_{15}		
Scheme	1	2	3	1	2	3
WT_{11}	0.65 / 2.3	4.1 / 10.5	0.5 / 2	0.1 / 0.5	1.2 / 1.9	0.05 / 0.3
WT_{12}	0.23 / 1.2	3 / 6.4	0.2 / 1.1	0.02 / 0.1	1.4 / 3	0.02 / 0.07
WT_{13}	0.2 / 0.9	3.5 / 7.8	0.2 / 0.8	0.03 / 0.12	1.1 / 3.4	0.03 / 0.07
WT_{14}	0.07 / 0.38	2.7 / 7.4	0.07 / 0.3	0.05 / 0.12	1.4 / 3.1	0.06 / 0.11
WT_{15}	0.03 / 0.11	1 / 3.3	0.04 / 0.11	0.44 / 0.8	7.3 / 14.3	0.34 / 0.7
WT_{21}	-**	0.4 / 3	-	0 / 0.1	0.54 / 1.1	-
WT_{22}	-	0.04 / 0.2	-	-	0.5 / 1.3	-
WT_{23}	-	0.05 / 0.4	-	-	0.6 / 2.4	-
WT_{24}	-	0.16 / 1.4	-	-	0.4 / 1.5	-
WT_{25}	-	0.1 / 1.2	-	-	0.7 / 1.3	-

* E_{sa} is presented as x_1/x_2 where x_1 and x_2 are E_{sa} computed for ρ_1 and ρ_2, respectively.
** (-) means E_{sa} is less than 0.01 (kJ) for both ρ_1 and ρ_2.

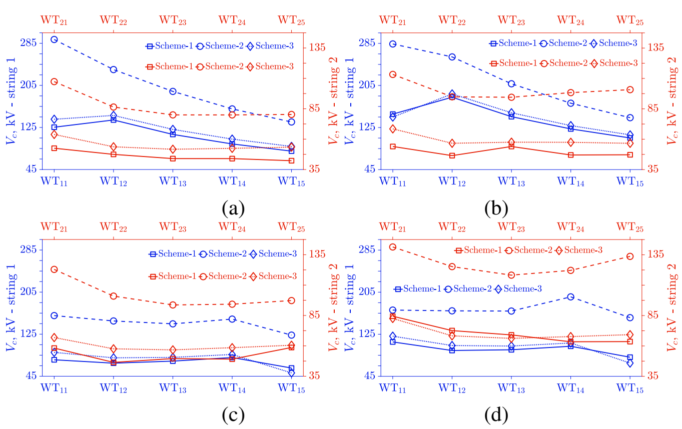

Fig. 14. Waveforms of V_c. (Left column: ρ_1; right column: ρ_2.) (a), (b) FRS to WT_{11}; (c), (d) FRS to WT_{15}.

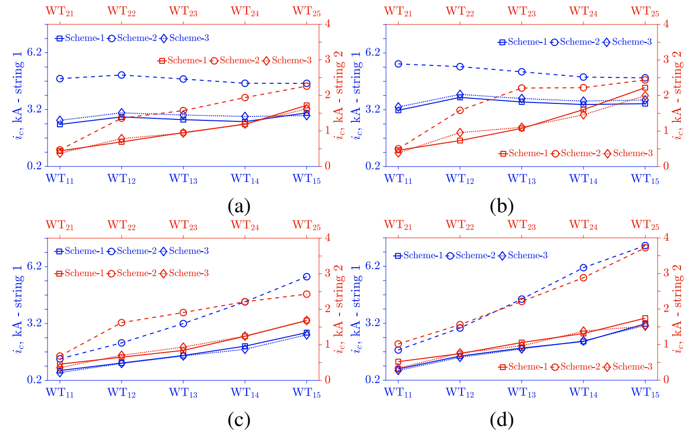

Fig. 15. Waveforms of i_c. (Left column: ρ_1; right column: ρ_2.) (a), (b) FRS to WT_{11}; (c), (d) FRS to WT_{15}.

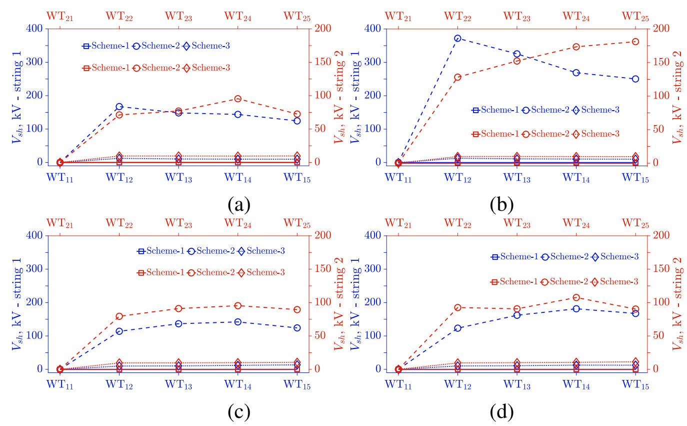

Fig. 16. Waveforms of V_{sh}. (Left column: ρ_1; right column: ρ_2.) (a), (b) FRS to WT_{11}; (c), (d) FRS to WT_{15}.

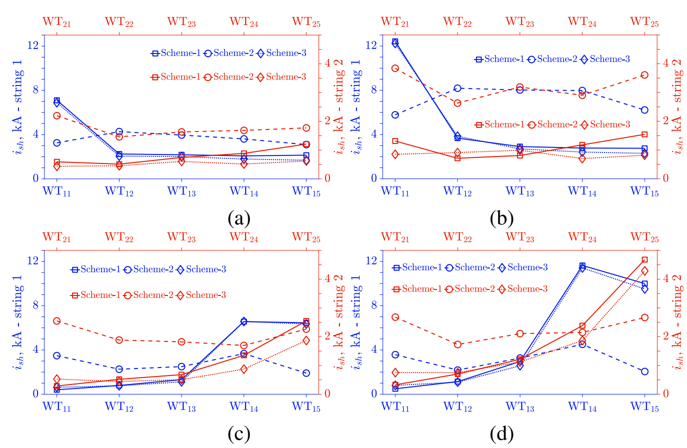

Fig. 17. Waveforms of i_{sh}. (Left column: ρ_1; right column: ρ_2.) (a), (b) FRS to WT_{11}; (c), (d) FRS to WT_{15}.

arresters for WT vertical and horizontal underground cables so as to assure that flow of DCWF return currents is through grounding system rather than cable sheath. Those arresters suppress also the seriously arose sheath voltages during direct lightning incidents that is likely destructive for cables insulation and interface converters. To counteract the high soil resistivity, the entire grounding system of DCWF is boosted by counterpoises network to render a low-impedance discharge path for surge currents. Furthermore, the proposed scheme can also be applied to offshore DCWFs and other WTG types. A detailed system that appropriately mimics models of cables, grounding system and WTG converters is constructed to assess the efficacy of the proposed scheme. Obtained results have demonstrated the capability of the proposed scheme to cease flow of return currents via sheath and mitigate higher

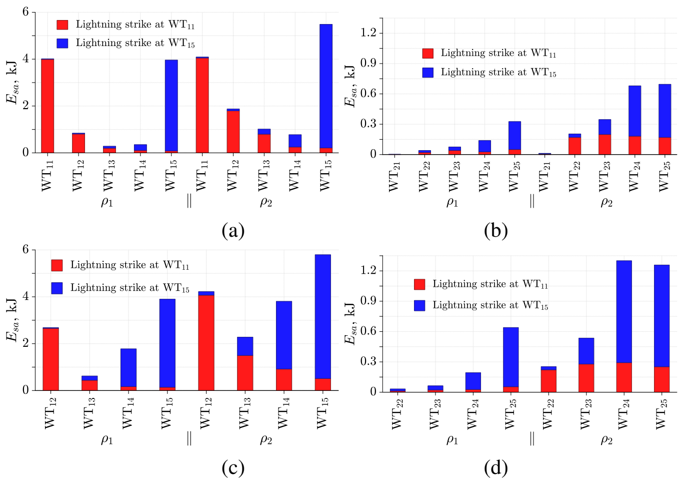

Fig. 18. E_{sa} for SAs in scheme-3. (Left column: string-1; right column: string-2) (a), (b) E_{sa} of SA_{vs}; (c), (d) E_{sa} of SA_{hs}.

TABLE V
ENERGY CONSUMED, E_{sa} IN (KJ) FOR SHEATH ARRESTER SA_S.

FRS	SA_{vs}				SA_{hs}			
	WT_{11}		WT_{15}		WT_{11}		WT_{15}	
	ρ_1	ρ_2	ρ_1	ρ_2	ρ_1	ρ_2	ρ_1	ρ_2
WT_{11}	4	4.1	0.01	0.04				
WT_{12}	0.8	1.8	0.04	0.08	2.7	4.1	0.03	0.15
WT_{13}	0.2	0.8	0.08	0.2	0.4	1.5	0.2	0.78
WT_{14}	0.1	0.25	0.25	0.5	0.2	0.9	1.6	2.9
WT_{15}	0.08	0.2	3.9	5.3	0.14	0.5	3.8	5.3
WT_{21}	-	-	-	-				
WT_{22}	0.02	0.17	0.02	0.03	0.01	0.2	0.02	0.03
WT_{23}	0.04	0.2	0.03	0.12	0.02	0.3	0.04	0.26
WT_{24}	0.03	0.18	0.1	0.49	0.03	0.3	0.17	1
WT_{25}	0.05	0.17	0.3	0.53	0.05	0.25	0.6	1

transient voltages and currents during lightning compared to other operational schemes. As the suggested arresters are adequately away from their thermal capacity during direct lightning strikes, the proposed scheme is thus economical on the long-run for such platforms.

REFERENCES

[1] K. Park and Z. Chen, "Control and dynamic analysis of a parallel-connected single active bridge dc–dc converter for DC-grid wind farm application," *IET Power Electron.*, vol. 8, no. 5, pp. 665–671, 2015.

[2] ——, "A double uneven power converter-based DC–DC converter for high-power DC grid systems," *IEEE Trans. Ind. Electron.*, vol. 62, no. 12, pp. 7599–7608, 2015.

[3] S. Abulanwar, A. Ghanem, M. E. Rizk, and I. Ismael, "Mitigation of DC wind farm power fluctuations based battery energy storage system," in *2019 21st International Middle East Power Systems Conference (MEPCON)*. IEEE, 2019, pp. 1089–1094.

[4] L. Cai, U. Karaagac, and J. Mahseredjian, "Simulation of startup sequence of an offshore wind farm with MMC-HVDC grid connection," *IEEE Trans. Power. Del.*, vol. 32, no. 2, pp. 638–646, 2016.

[5] Z. Wang and H. Li, "An integrated three-port bidirectional DC–DC converter for PV application on a DC distribution system," *IEEE Trans. Power Electron.*, vol. 28, no. 10, pp. 4612–4624, 2012.

[6] G. Guo, H. feng Wang, Q. Song, J. Zhang, T. Wang, B. Ren, and Z. Wang, "HB-and FB-MMC based onshore converter in series-connected offshore wind farm," *IEEE Trans. Power Electron.*, 2019.

[7] M. Guan, "A series-connected offshore wind farm based on modular dual-active-bridge (DAB) isolated dc-dc converter," *IEEE Trans. Energy Convers.*, 2019.

[8] S. Muyeen, R. Takahashi, and J. Tamura, "Operation and control of HVDC-connected offshore wind farm," *IEEE Trans. Sustain. Energy*, vol. 1, no. 1, pp. 30–37, 2010.

[9] A. C. Garolera, S. F. Madsen, M. Nissim, J. D. Myers, and J. Holboell, "Lightning damage to wind turbine blades from wind farms in the US," *IEEE Trans. Power. Del.*, vol. 31, no. 3, pp. 1043–1049, 2016.

[10] Y. Yasuda, N. Uno, H. Kobayashi, and T. Funabashi, "Surge analysis on wind farm when winter lightning strikes," *IEEE Trans. Energy Convers.*, vol. 23, no. 1, pp. 257–262, 2008.

[11] IEC, "61400-24 wind turbines-part 24: Lightning protection," International Electrotechnical Commission, Geneva, Switzerland, 2010.

[12] R. Hoerauf, "Considerations in wind farm grounding designs," *IEEE Trans. Ind. Appl.*, vol. 50, no. 2, pp. 1348–1355, 2013.

[13] M. E. Rizk, F. Mahmood, M. Lehtonen, E. A. Badran, and M. H. Abdel-Rahman, "Investigation of lightning electromagnetic fields on underground cables in wind farms," *IEEE Trans. Electromagn. Compat.*, vol. 58, no. 1, pp. 143–152, 2015.

[14] R. G. Deshagoni, T. Auditore, R. Rayudu, and C. P. Moore, "Factors determining the effectiveness of a wind turbine generator lightning protection system," *IEEE Trans. Ind Appl.*, vol. 55, no. 6, pp. 6585–6592, 2019.

[15] S. Sekioka, H. Otoguro, and T. Funabashi, "A study on overvoltages in windfarm caused by direct lightning stroke," *IEEE Trans. Power. Del.*, vol. 34, no. 2, pp. 671–679, 2018.

[16] A. Ametani and T. Kawamura, "A method of a lightning surge analysis recommended in Japan using EMTP," *IEEE Trans. Power. Del.*, vol. 20, no. 2, pp. 867–875, 2005.

[17] F. Heidler and J. Cvetić, "A class of analytical functions to study the lightning effects associated with the current front," *Eur. Trans. Electr. Power*, vol. 12, no. 2, pp. 141–150, 2002.

[18] A. De Conti and S. Visacro, "Analytical representation of single-and double-peaked lightning current waveforms," *IEEE Trans. Electromagn. Compat.*, vol. 49, no. 2, pp. 448–451, 2007.

[19] T. H. Thang, Y. Baba, N. Nagaoka, A. Ametani, N. Itamoto, and V. A. Rakov, "FDTD simulation of insulator voltages at a lightning-struck tower considering ground-wire corona," *IEEE Trans. Power Del.*, vol. 28, no. 3, pp. 1635–1642, 2013.

[20] M. E. M. Rizk, M. Lehtonen, Y. Baba, and S. Abulanwar, "Performance of large-scale grounding systems in thermal power plants against lightning strikes to nearby transmission towers," *IEEE Trans. Electromagn. Compat.*, vol. 61, no. 2, pp. 400–408, April 2019.

[21] E. D. Sunde, *Earth conduction effects in transmission systems*. New York: Dover Publications Inc., 1968.

[22] L. Grcev and M. Popov, "On high-frequency circuit equivalents of a vertical ground rod," *IEEE Trans. Power Del.*, vol. 20, no. 2, pp. 1598–1603, 2005.

[23] M. E. M. Rizk, M. Lehtonen, Y. Baba, and A. Ghanem, "Protection against lightning-induced voltages: Transient model for points of discontinuity on multiconductor overhead line," *IEEE Trans. Electromagn. Compat.*, pp. 1–10, 2019.

[24] ABB, "XLPE cable systems. users guide," 2013.

[25] P. Pinceti and M. Giannettoni, "A simplified model for Zinc Oxide surge arresters," *IEEE Trans. Power Del.*, vol. 14, no. 2, pp. 393–398, 1999.

[26] ABB, "Technical surge arrester data," *Available on https://new.abb.com/high-voltage/surge-arresters*, 2018.

[27] A. Ghanem, S. Abulanwar, M. Rizk, and M. Rashed, "A proposed controller and stability analysis for DFIG to suppress stator flux oscillations during autonomous operation," *IET Renew. Power Gener.*, 2019.

[28] N. P. Strachan and D. Jovcic, "Stability of a variable-speed permanent magnet wind generator with weak AC grids," *IEEE Trans. Power. Del.*, vol. 25, no. 4, pp. 2779–2788, 2010.

[29] C. Wei, Z. Zhang, W. Qiao, and L. Qu, "An adaptive network-based reinforcement learning method for MPPT control of PMSG wind energy conversion systems," *IEEE Trans. Power Electron.*, vol. 31, no. 11, pp. 7837–7848, 2016.

Mohammad E. M. Rizk (M'19) received the B.Sc. and M.Sc. degrees in Electrical Engineering from Mansoura University, Mansoura, Egypt in 2007 and 2011 respectively, and the D.Sc. degree from Aalto University, Espoo, Finland, in 2016. He joined Aalto University as a postdoctoral researcher at the Department of Electrical Engineering and Automation in 2017. Currently, he is Assistant Professor of electrical engineering at Mansoura University. His research interests include power system transients, lightning overvoltages in power systems and transient electromagnetic fields.

Sayed Abulanwar (S'12-M'16) received the B.Sc. and M.Sc. degrees in Electrical Engineering from Mansoura University, Mansoura, Egypt in 2005 and 2010, respectively. In 2016, he received the Ph.D. degree from Aalborg University, Aalborg, Denmark. Currently, he is Assistant Professor of electrical engineering at Mansoura University. His research interests include wind turbine control, HVDC systems, and transients in power systems.

Abdelhady Ghanem (M'18) received the B.Sc., M.Sc., and Ph.D. degrees, all in electrical engineering, from Mansoura University, Mansoura, Egypt, in 2006, 2011, and 2017, respectively. Since 2006, he has been employed by the Electrical Engineering Department at Mansoura University, where he is now an Assistant Professor. He joined University of Nottingham, Nottingham, U.K., as an Occasional PhD Student (Joint Supervision Scheme between Mansoura University and University of Nottingham) from February 2015 to May 2017. His research interests include electrical systems modelling, renewable power generation, power system analysis and control, grid connected power electronics converters, and stability analysis.

Zhe Chen (M'95–SM'98–F'19) received the B.Eng. and M.Sc. degrees all in Electrical Engineering from Northeast China Institute of Electric Power Engineering, Jilin City, China, MPhil in Power Electronic, from Staffordshire University, England and the Ph.D. degree in Power and Control, from University of Durham, England.

Dr Chen has been a full Professor with the Department of Energy Technology, Aalborg University, Denmark since 2002. He is the leader of Wind Power System Research program at the Department of Energy Technology, Aalborg University and the Danish Principle Investigator for Wind Energy of Sino-Danish Centre for Education and Research.

His research areas are power systems, power electronics and electric machines; and his main current research interests are wind energy and modern power systems. He has led and participated in many research and industrial projects and has been a panel member of research funding evaluation committees in many EU countries.

Dr Chen is an Associate Editor of the IEEE Transactions on Power Electronics, a member of editorial boards for many international journals, a Fellow of the Institution of Engineering and Technology (London, U.K.), and a Chartered Engineer in the U.K.